Defining modulatory inputs into CNS neuronal subclasses by functional pharmacological profiling

Shrinivasan Raghuraman[a,1], Alfredo J. Garcia[b,c,1], Tatiana M. Anderson[b,c,d], Vernon D. Twede[a], Kigen J. Curtice[a], Kevin Chase[a], Jan-Marino Ramirez[b,c,d], Baldomero M. Olivera[a,2], and Russell W. Teichert[a,2]

[a]Department of Biology, University of Utah, Salt Lake City, UT 84112; [b]Center for Integrative Brain Research, Seattle Children's Research Institute, [c]Department of Neurological Surgery and Pediatrics, and [d]Neurobiology Graduate Program, The University of Washington School of Medicine, Seattle, WA 98101

Contributed by Baldomero M. Olivera, March 14, 2014 (sent for review January 13, 2014)

Previously we defined neuronal subclasses within the mouse peripheral nervous system using an experimental strategy called "constellation pharmacology." Here we demonstrate the broad applicability of constellation pharmacology by extending it to the CNS and specifically to the ventral respiratory column (VRC) of mouse brainstem, a region containing the neuronal network controlling respiratory rhythm. Analysis of dissociated cells from this locus revealed three major cell classes, each encompassing multiple subclasses. We broadly analyzed the combinations (constellations) of receptors and ion channels expressed within VRC cell classes and subclasses. These were strikingly different from the constellations of receptors and ion channels found in subclasses of peripheral neurons from mouse dorsal root ganglia. Within the VRC cell population, a subset of dissociated neurons responded to substance P, putatively corresponding to inspiratory pre-Bötzinger complex (preBötC) neurons. Using constellation pharmacology, we found that these substance P-responsive neurons also responded to histamine, and about half responded to bradykinin. Electrophysiological studies conducted in brainstem slices confirmed that preBötC neurons responsive to substance P exhibited similar responsiveness to bradykinin and histamine. The results demonstrate the predictive utility of constellation pharmacology for defining modulatory inputs into specific neuronal subclasses within central neuronal networks.

calcium imaging | NK1 receptor | glutamate | acetylcholine | conotoxin

Progress in understanding the mammalian brain has been impeded by the extraordinary complexity of cell types comprising the circuitry and the difficulty in bridging different levels of biological organization from the molecular to the cellular and systems level (1–4). Systems neuroscientists study the circuitry and high-level functions of the brain, whereas molecular neuroscientists study the molecular components. The large divide between these two branches of neuroscience clearly needs to be bridged to understand fully neuronal and behavioral functions in health and disease. To this end, we recently demonstrated an experimental approach we call "constellation pharmacology" to identify different neuronal subclasses by the combinations (constellations) of receptors and ion channels functionally expressed in each subclass (5–8). This experimental approach initially was applied to somatosensory neurons of the peripheral nervous system (PNS). In the present study, we use constellation pharmacology to identify neuronal subclasses of the CNS and to characterize these subclasses at the network level. Specifically, we have used constellation pharmacology to define the diverse cell types found in the mouse ventral respiratory column (VRC) and surrounding brainstem tissue.

The VRC contains a variety of neurons that are active during either inspiratory or expiratory phases of breathing. One key network within the VRC is the pre-Bötzinger complex (preBötC), which contains the circuitry essential for generating the respiratory rhythm (9–12). This network of inspiratory neurons is heterogeneous, encompassing neurons with unique pharmacological profiles (13–17). Moreover, the tissue immediately surrounding the preBötC also contains neuronal networks important to cardiovascular control, such as cardiac parasympathetic vagal neurons of the nucleus ambiguus and noradrenergic neurons of the A2/C2 region (18, 19). This anatomical convergence of networks responsible for respiratory and cardiovascular control creates an avenue through which different control elements may coordinate and couple (20) but also produces a cellular population that is heterogeneous in the responsiveness to neuromodulation.

Here we used constellation pharmacology to identify three major cell classes from the VRC and surrounding tissue. Each of these major cell classes encompasses additional subclasses that exhibit unique pharmacological profiles. We focused on one specific neuronal subclass that is responsive to substance P because substance P is an established modulator of inspiratory preBötC neurons (16). Constellation pharmacology suggested that substance P-responsive inspiratory neurons also would be responsive to histamine and bradykinin. This hypothesis was confirmed in the acute brainstem slice. Thus, this study demonstrates the utility of constellation pharmacology for investigating cell-specific constellations of receptors and ion channels expressed within neuronal and glial subclasses of the mouse brainstem and the broader potential for bridging molecular and systems neuroscience at the cellular level.

Results

Dissociated VRC Cell Cultures. We prepared cultures of dissociated VRC cells as described in *SI Materials and Methods*. Briefly, for each culture, we prepared a brainstem slice ~200 microns thick, at the level of the preBötC, from a mouse at postnatal day 7 or 8 (P7-8). We followed the same experimental approach and same protocols that we developed for producing rhythmically active

Significance

We functionally profiled cells from a locus of the mouse brainstem that contains the neuronal network responsible for generating breathing patterns. By uncovering cell-specific constellations (i.e., distinctive combinations of receptors and ion channels that define each cell type), we identified specific neuronal classes and subclasses within the network. We discovered neuromodulators affecting the activity of specific neuronal subclasses within the functional network. This study provides proof-of-principle that a pharmacological strategy for altering the activity of a specific type of neuron can be developed which has potential as a parallel or complementary approach to genetic strategies for functionally perturbing a specific neuronal cell type in vivo. Additionally, unlike genetic approaches, this pharmacological approach is directly applicable to nonmodel organisms.

Author contributions: J.-M.R., B.M.O., and R.W.T. designed research; S.R., A.J.G., T.M.A., V.D.T., and K.J.C. performed research; S.R., A.J.G., K.C., and R.W.T. analyzed data; and A.J.G., J.-M.R., B.M.O., and R.W.T. wrote the paper.

The authors declare no conflict of interest.

[1]S.R. and A.J.G. contributed equally to this work.

[2]To whom correspondence may be addressed. E-mail: olivera@biology.utah.edu or Russ.Teichert@utah.edu.

This article contains supporting information online at www.pnas.org/lookup/suppl/doi:10.1073/pnas.1404421111/-/DCSupplemental.

brainstem slice preparations (15, 17, 21). The region containing the preBötC and surrounding VRC was microdissected from the brainstem slice; then the cells were dissociated by enzymatic (trypsin) and mechanical methods. Cells were cultured overnight before calcium-imaging experiments were performed.

Fig. S1 shows images of dissociated VRC cell cultures of inadequate, optimal, and excessive density. In our hands, the optimal plating density was ~800 cells/mm^2 (not all cells survive). This plating density allowed us to perform calcium-imaging experiments in which we could monitor the individual responses of more than 100 cells simultaneously while avoiding an excessive number of cells that overlapped or made contact with neighboring cells. This optimal density enabled us to report the intrinsic responses of individual cells confidently in this study.

Calcium Imaging. Fig. S1 exemplifies a VRC cell culture that was used for a calcium-imaging experiment. The images in Fig. S1 *D–G* show the same field of view. Fig. S1*D* is bright-field image. A fluorescence image of the same cells loaded with Fura-2-AM dye (380-nm excitation and 510-nm emission) is shown in Fig. S1*E*. Fig. S1*F* is a pseudocolored ratiometric image of cells loaded with Fura-2-AM dye at rest. The ratio of fluorescence intensities at 510-nm emission, when excited alternately with 340-nm and 380-nm light, provides a relative measure of cytosolic calcium concentration, $[Ca^{2+}]_i$. Fig. S1*G* is a ratiometric image taken immediately after a stimulus to which a subset of the cells in the culture responded with an increase in $[Ca^{2+}]_i$.

The essence of the constellation pharmacology strategy is to probe a heterogeneous population of dissociated cells with a panel of selective pharmacological agents, among other physicochemical perturbations, and to monitor simultaneously the individual responses of more than 100 cells by calcium imaging. By monitoring the different response phenotypes, we can parse cell populations into major cell classes and minor subclasses.

Pharmacological Profiling of VRC Cells. Fig. 1 exemplifies calcium-imaging traces from selected VRC cells in response to a set of receptor agonists and to depolarization by a high concentration (e.g., 100 mM) of extracellular potassium (high $[K^+]_o$). Abbreviations and concentrations for each of the pharmacological agents and other cellular perturbations used in this study are summarized in Table 1. Three major classes of cells within these cultures could be differentiated by their distinct response profiles.

The first major cell class, class A, was defined by responsiveness to high $[K^+]_o$ and by the lack of responses to a panel of receptor agonists (Fig. 1*A* and Table 2). The second major cell class, class B, was defined by responsiveness to high $[K^+]_o$ and one or more receptor agonists tested (Fig. 1*B* and Table 2). Notably, responsiveness to glutamate was excluded as a criterion for classifying cells, because ~75% of both class A and class B cells responded to glutamate. However, only class B cells responded to the other receptor agonists (Table 2). In fact, the majority of class B cells responded to each of the receptor agonists, with the exceptions of the neuropeptides substance P and bradykinin, to which a minority of the class B cells responded (Table 2).

On average, class A cells responded to depolarization by high $[K^+]_o$ with large, transient increases in $[Ca^{2+}]_i$ (Fig. 1*A* and Table 2), indicating that they express high levels of voltage-gated calcium channels as is characteristic of neurons. On average, class B cells responded less strongly than class A cells to depolarization by high $[K^+]_o$ (Fig. 1*B* and Table 2). This difference was statistically significant (P value = 0.001, Student t test). At present it is unclear whether class B cells are all neurons or are a mixed population of neurons and glia.

The third major cell class, class C, comprises putative nonneuronal cells (glial cells and potentially other nonneuronal cells) that did not respond to depolarization by high $[K^+]_o$ or responded very weakly (i.e., a change in 340/380-nm ratio <0.1) (Fig. 1*C* and Table 2), suggesting that, unlike neurons, they do not express voltage-gated calcium channels or express these channels at very low levels. A small minority of class C cells responded to each of the receptor agonists tested (Table 2). However, when we reduced the resting $[K^+]_o$ from 3 mM to 0.2 mM, 30% of the class C cells responded with an increase in $[Ca^{2+}]_i$ (Fig. S2). Such responses (putatively mediated by $K_{ir}4.1$) have been shown to be specific to astrocytes in the VRC (22, 23). This evidence supports the hypothesis that many class C cells are glial (astrocytes and other glial cells). Furthermore, none of the class A cells responded to 0.2 mM $[K^+]_o$, thus supporting the hypothesis that class A cells are all neurons. However, 6% of the class B cells responded to 0.2 mM $[K^+]_o$, suggesting that some of the class B cells are astrocytes.

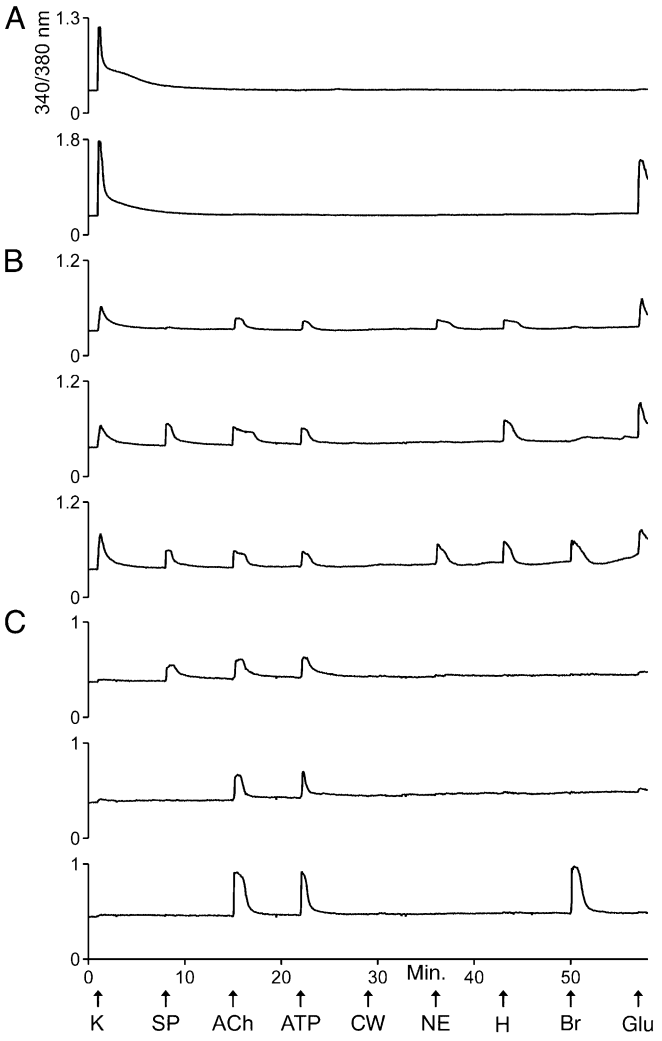

Fig. 1. Examples of calcium-imaging traces from dissociated VRC cells in culture. Each trace is the response of a single cell to the experimental protocol depicted at the bottom of the figure. In each experimental trial, the individual responses of >100 cells were monitored simultaneously. The *x*-axis and experimental protocol at the bottom of the figure apply to all traces in the figure. The units of the *x*-axis are time in minutes. The arrows identify time points when various types of stimuli were applied to the cells for 15 s. The abbreviations for these stimuli are defined in Table 1. "CW" represents a control wash, i.e., the replacement of bath solution (artificial CSF, aCSF) with identical bath solution. The *y*-axis for each trace is the ratio of fluorescence intensities obtained at 510-nm emission from the alternating excitation by 340-nm or 380-nm light. It is a measure of relative changes in $[Ca^{2+}]_i$. (*A*) Examples of traces from class A cells. Both cells responded strongly to depolarization by high $[K^+]_o$, but only one responded to glutamate with an increase in $[Ca^{2+}]_i$. (*B*) Examples of traces from class B cells. Notably, these cells responded less strongly than class A cells to high $[K^+]_o$. They typically responded to several receptor agonists, as shown. (*C*) Examples of traces from class C cells. These cells either did not respond to depolarization by high $[K^+]_o$ or responded very weakly.

Table 1. Abbreviations of compounds cited in figures and tables

Abbreviation	Compound	Working concentration
ACh	Acetylcholine	1 mM
ArIB	α-Conotoxin ArIB[V11L;V16D]	200 nM
ATP	Adenosine 5′ triphosphate	20 μM
Br	Bradykinin	10 μM
CW	Control Wash	NA
Glu	Glutamate	300 μM
H	Histamine	50 μM
K	$[K^+]_o$	100 mM
NE	Norepinephrine	20 μM
NMDA	*N*-methyl-D-aspartate and	100 μM
D-ser	D-serine	10 μM
PNU	PNU-120596	5 μM
SP	Substance P	1 μM

Cluster Analysis of VRC Cells. With the eight stimuli shown in Fig. 1, it theoretically is possible to identify 256 unique cell-response profiles, but 103 unique response profiles actually were observed. We first grouped these 103 response profiles into three broad cell classes, A, B, and C, as described above and as shown in Table 2. We then performed cluster analysis to determine whether these broad cell classes were supported by an unbiased data analysis. The cluster analysis included 1,586 cells, representing the 103 unique response profiles, which clustered robustly into three broad cell classes in all 500 bootstrap trials. These broad cell classes were consistent with our original designations of cell classes A, B, and C.

As a lower bound on the number of unique cell profiles robustly identified, we estimated the number of clusters required to explain most of the variation in cell responses. The cluster analysis summarized in Table S1 grouped cells into 36 clusters that explain 99% of the cell responses. We then sorted those 36 clusters from Table S1 into broader groups that essentially correspond to our original assignments of class A cells (the top two clusters), class B cells (the middle 24 clusters), and class C cells (the bottom 10 clusters). Notably, for each cluster shown in Table S1, the predominant response profiles (the prototype response profile) and the mean responses to depolarization by high $[K^+]_o$ (the mean K^+ response) agree with these broader cell class designations.

Comparison of VRC and DRG cells. For direct comparison with VRC cells, we conducted the profiling protocol shown in Fig. 1 with cultures of dorsal-root ganglion (DRG) cells from mice of the same age (P7-8). Table 2 shows the direct comparison between VRC and DRG cells in response to the same panel of pharmacological agents. We divided DRG cells into a combined class A/B group and a separate class C group. The distinction between class A and B cells that was obvious in the VRC was not evident in the DRG. Furthermore, in the DRG, the cell bodies of the neurons are morphologically distinct from the other cell bodies in the culture: The neuronal cell bodies are larger in diameter than the nonneuronal cell bodies and are rounder than the cell bodies of the satellite glial cells, which are relatively flat and elongated (24). Therefore, we can conclude that in DRG cultures the class A/B cells are neurons and the class C cells are various nonneuronal cells.

There are several notable points of comparison and contrast between VRC and DRG cultures from P7-8 mice (Table 2): A very high percentage of the class C cells in DRG cultures responded to ATP, in contrast to the low percentage of ATP-responsive class C cells in VRC cultures. In VRC cultures, the majority of the class B cells and a small subset of class C cells responded to norepinephrine with an increase in $[Ca^{2+}]_i$, but almost none of the DRG cells responded to norepinephrine in this way. In VRC cultures, the majority of class A and B cells responded to glutamate, in contrast to the low percentage of glutamate-responsive class A/B cells in DRG cultures. A qualitative assessment of the glutamate responses indicated that the glutamate responses in VRC cells were relatively large compared with the very small responses observed in DRG cells. Other interesting points of comparison and contrast are shown in Table 2.

Acetylcholine-Receptor Expression in VRC Cell Classes. In addition to the experimental protocols shown in Fig. 1 and Fig. S2, we investigated the expression of acetylcholine (ACh) receptors (AChRs) in VRC cells (Fig. S3). We observed that responses to ACh were blocked by atropine, suggesting that these responses were mediated primarily by muscarinic acetylcholine receptors (mAChRs) and not nicotinic acetylcholine receptors (nAChRs) (Fig. S3). When the cells were preincubated with a positive allosteric modulator of α7 nAChRs, PNU-120596 (PNU), then a different subset of cells responded to ACh. Notably, α7 nAChRs desensitize very rapidly upon application of ACh (25). Such rapid desensitization may prevent a measurable increase in $[Ca^{2+}]_i$ in the absence of PNU. To confirm that the ACh responses in the presence of PNU were mediated by α7 nAChRs, we blocked the responses with the highly subtype-selective blocker of α7 nAChRs, α-conotoxin ArIB[V11L;V16D] (Fig. S3) (26).

As shown in Fig. S3, we divided VRC cells into classes A, B, and C, on the basis of their responses to high $[K^+]_o$, ACh (before PNU application), substance P (as shown in Fig. S3), and norepinephrine. Cells were classified as class A if they responded only to high $[K^+]_o$ and as class B if they responded to high $[K^+]_o$ and to ACh (before PNU application) or substance P or

Table 2. Summary of responses from the profiling experiments depicted in Fig. 1

	Criteria for classification				% responsive cells in each cell class						
Cell class	Average response to 100 mM $[K^+]_o$ ± SD	Responsiveness to pharmacological compounds	Total cells	% of total cells	SP	ACh	ATP	NE	H	Br	Glu
Ventral respiratory column (P7-8 mouse)											
Class A	0.8 ± 0.4	Responsive to glutamate only and response to 100 mM $[K^+]_o \geq 0.1$	220	13	0	0	0	0	0	0	78
Class B	0.3 ± 0.2	Responsive to other receptor agonists and response to 100 mM $[K^+]_o \geq 0.1$	574	33	8	91	68	65	74	35	76
Class C	0.0 ± 0.0	Response to 100 mM $[K^+]_o < 0.1$	965	55	1	6	8	4	5	6	6
Dorsal root ganglia (P8 mouse)											
Class A/B	Responsive	Response to 100 mM $[K^+]_o \geq 0.1$	787	32	0	7	76	1	6	27	3
Class C	0	Response to 100 mM $[K^+]_o < 0.1$	1,673	68	0	7	86	0	0	5	0

The average response to 100 mM $[K^+]_o$ ± SD is a relative measure of the change in $[Ca^{2+}]_i$ elicited by 100 mM $[K^+]_o$ (i.e., change in the 340/380-nm ratio shown in figures and described in *SI Materials and Methods*). Larger numbers indicate a greater response or greater relative change in $[Ca^{2+}]_i$ elicited by high $[K^+]_o$. The VRC dataset was compiled from five independent experimental trials using cells prepared separately from four different mice. The DRG dataset was compiled from six independent experimental trials using cells prepared separately from two different mice. ACh, acetylcholine; Br, bradykinin; Glu, glutamate; H, histamine; NE, norepinephrine; SP, substance P.

NEUROSCIENCE

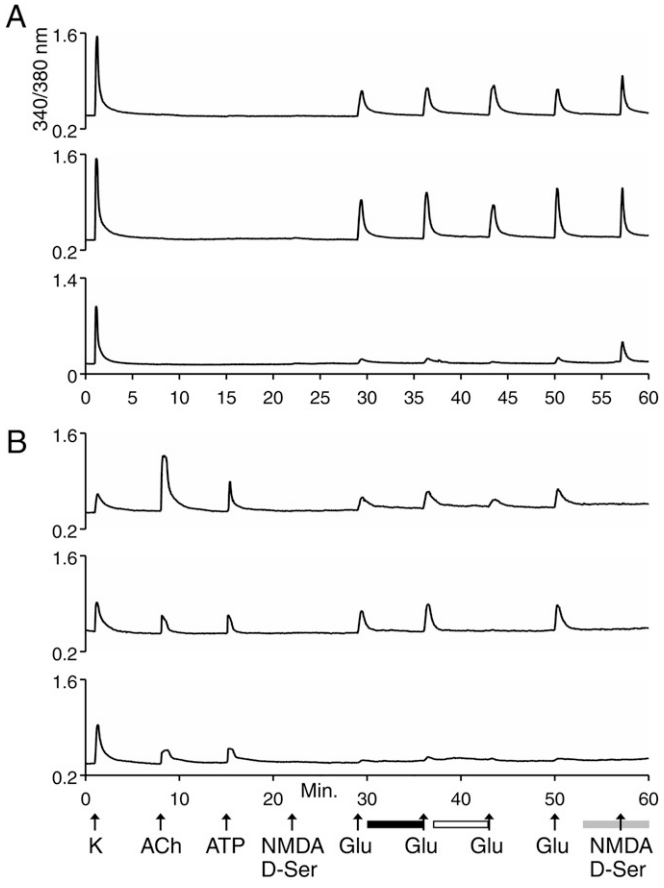

C

Cell Class	Avg Resp. to 100 mM $[K^+]_o$	% of Total Cells	% of responsive cells in each cell class: NMDA-R	Non-NMDA-R	Glu Resp. Blocked by CNQX (>5% block)	Avg %block by CNQX(S.D.)
A	1.2	7%	49%	51%	84%	60% (31%)
B	0.3	30%	6%	84%	99%	81% (24%)
C	0.0	63%	0%	1%	99%	89% (16%)

Fig. 2. Examples of calcium-imaging traces from experiments investigating glutamate receptors in dissociated VRC cells presented as in Fig. 1. (*A*) Examples of traces from class A cells. (*B*) Examples of traces from class B cells. In *A* and *B* there was no response to NMDA/D-ser in the presence of Mg^{2+} at minute 22 (because Mg^{2+} blocks NMDA receptors without a depolarizing stimulus; compare with NMDA/D-ser application at minute 57 in the absence of Mg^{2+}), indicating that the subsequent responses to 300 μM glutamate were mediated by AMPA/kainite receptors and/or metabotropic glutamate receptors. The black horizontal bar below the *x*-axis indicates the presence of 100 μM AP5 (an NMDA receptor inhibitor) in the bath. The presence of 100 μM AP5 did not block the response to the second application of 300 μM glutamate, confirming that these responses were not mediated by NMDA receptors. The open horizontal bar below the *x*-axis indicates the presence of 10 μM CNQX (an AMPA/kainite receptor inhibitor) in the bath. In general, CNQX partially blocked glutamate-elicited responses, indicating expression of a mix of AMPA/kainite receptors and metabotropic glutamate receptors. The gray horizontal bar below the *x*-axis indicates the time point when the bath solution (aCSF) was changed to Mg^{2+}-free aCSF. The application of NMDA/D-ser in the absence of Mg^{2+} demonstrated that about half of class A cells but only a small minority of class B cells expressed NMDA receptors. (*C*) Compilation of data for class A and B cells. This dataset was compiled for 2,483 cells from eight independent experimental trials, using cells prepared separately from five different mice. Notably, there are some minor discrepancies between the data compiled in *C* from the experimental protocol depicted in *A* and *B* and the data compiled in Table 2 from the experimental protocol depicted in Fig. 1; these discrepancies demonstrate a range of experimental variability.

norepinephrine. Class C cells were determined by the same criterion used in Table 2, a change in the 340/380-nm ratio <0.1 in response to high $[K^+]_o$. On average, the class A cells exhibited greater responses to high $[K^+]_o$ than class B cells, as expected and as demonstrated in Fig. S3*D*. None of the class A cells responded to ACh before the application of PNU. However, after preincubation with PNU, the majority of class A cells (66%) began to respond to ACh, indicating that they express functional α7 nAChRs (Fig. S3 *A* and *D*). In contrast to class A cells, the majority of class B cells (73%) responded to ACh before PNU application. Those responses were blocked by atropine, indicating that the majority of class B cells express functional mAChRs (Fig. S3 *B* and *D*).

Glutamate-Receptor Expression in VRC Cell Classes. For the following experiments exploring glutamate-receptor expression, cells were parsed into classes A, B, and C by the following criteria: Cells were considered class A if they responded only to high $[K^+]_o$ and as class B if they responded to high $[K^+]_o$ and either ACh (in the absence of PNU) or ATP (Fig. 2). Class C cells were determined by the criterion used in Table 2, a change in 340/380-nm ratio <0.1 in response to high $[K^+]_o$. On average, the class A cells exhibited greater responses to high $[K^+]_o$ than class B cells, as expected and as demonstrated in Fig. 2*C*. Notably, approximately half of class A cells were found to express functionally NMDA receptors [see response to NMDA/D-serine (D-ser) at minute 57 in Fig. 2 *A* and *C*] and metabotropic glutamate receptors [for the portion of glutamate-elicited response not blocked by 6-cyano-7-nitroquinoxaline-2,3-dione (CNQX) in Fig. 2*A*], with or without detectable expression of non-NMDA (AMPA or kainate) receptors (for the portion of glutamate-elicited response blocked by CNQX in Fig. 2 *A* and *C*). The majority of class B cells functionally expressed AMPA and/or kainite receptors, but only a small minority expressed NMDA receptors (Fig. 2 *B* and *C*). Class C cells did not express NMDA receptors (Fig. 2*C*).

From Dissociated Cells to Functional Networks. Histological studies within the VRC demonstrate that neurokinin-1 receptors within this brainstem region are concentrated most densely at the level of the preBötC (27–29) and that the application of substance P to the preBötC stimulates both rhythmic network activity and excitability of synaptically isolated preBötC neurons in the brainstem slice preparation (16, 27). Thus, we focused on class B cells within our dissociated cell preparations that responded to substance P. Fig. 1*B* and Table S1 demonstrate that there were two main clusters (or subclasses) of substance P-responsive (class B) cells. Although both cellular subclasses were responsive to histamine, only one was responsive to bradykinin (Table S1). Thus, we hypothesized that histamine and bradykinin may directly modulate the activity of inspiratory preBötC neurons. Patch-clamp recordings were made from inspiratory preBötC neurons in rhythmically active brainstem slice preparations. When these neurons were identified in the functional network, they were isolated from fast synaptic transmission. Fig. 3 shows that histamine and bradykinin exhibited neuromodulatory effects in inspiratory neurons that also were responsive to substance P. Histamine or bradykinin changed firing patterns and increased the firing rate of many inspiratory neurons (Fig. 3). Moreover, as is consistent with the dissociated-cell experiments, substance P-responsive inspiratory neurons within the brainstem slice exhibited a variable sensitivity to bradykinin, as illustrated in the bradykinin response alone (Fig. 3 *B* and *C*) and when comparing

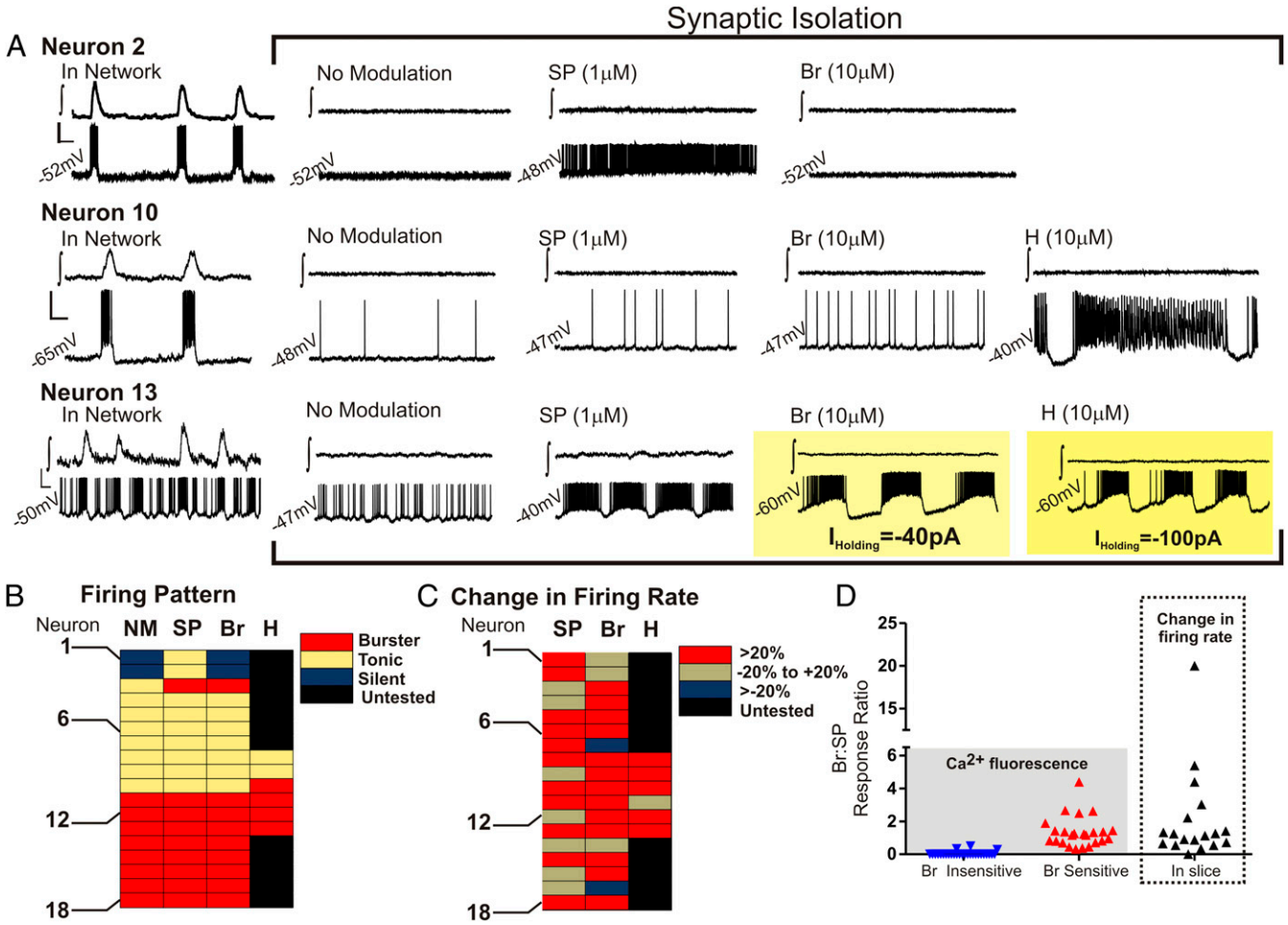

Fig. 3. The effects of substance P, bradykinin, and histamine on inspiratory neurons of the preBötC within a brainstem slice preparation. (*A*) Electrophysiology traces are shown in pairs from the preBötC population ($\int$, upper trace in each case) and a single inspiratory neuron of the preBötC (lower trace in each case) during synaptic isolation, without modulation, and in response to substance P (SP; 1 μM), bradykinin (Br; 10 μM), and histamine (H; 10 μM). (*Top*) Neuron 2 is silent in the absence of exogenous neuromodulation, is stimulated in the presence of substance P to exhibit a tonic firing pattern, is silent in the presence of bradykinin, and was not tested in the presence of histamine. (*Middle*) Neuron 10 is tonic in the absence of exogenous neuromodulation. Although both substance P and bradykinin stimulate a tonic firing rate, histamine changes the tonic firing pattern to a burster phenotype. (*Bottom*) Neuron 13 exhibits a burster phenotype in the absence of exogenous neuromodulation. Substance P stimulates the burster phenotype, whereas both bradykinin and histamine caused Neuron 13 to depolarize (>1.5 mV), requiring the injection of a hyperpolarizing current to prevent depolarization block. [Scale bars: 1 s (*x*-axis) and 20 mV (*y*-axis).] (*B–D*) Summaries of isolated inspiratory neurons ($n = 18$). These summaries demonstrate the diverse effects of substance P, bradykinin, and histamine on synaptically isolated inspiratory neurons. Examples of silent, tonic, and burster firing patterns are shown in *A*. (*B*) Firing pattern. (*C*) Change in firing rate. (*D*) Comparison of bradykinin responses as a ratio of substance P responses from individual substance P-sensitive dissociated cells (*Left*) and inspiratory preBötC neurons within the brainstem slice preparation (*Right*).

the individual bradykinin response with that of the respective substance P response (Fig. 3*D*).

Discussion

The results shown in Fig. 3 have two broad implications. (*i*) Constellation pharmacology can identify neuronal subclasses in dissociated cultures that maintain specific properties of neuronal subclasses within an organized network. (*ii*) Constellation pharmacology can be used to generate hypotheses that are testable, and in this case confirmed, within more intact systems. In conjunction with our prior studies of the PNS (5–8), this study suggests that constellation pharmacology may be applied productively to any locus of the CNS. Thus, our ultimate goal is to use constellation pharmacology broadly across different organisms, in different anatomical loci, and at different stages of development to characterize single cells by elucidating their cell-specific constellations of signaling proteins.

Previously, we reported a similar characterization of cells from mouse DRG (5–7), which we recently have extended to both trigeminal ganglia (TG) and DRG at different developmental stages (8). In the latter study, neurons from a genetic model organism (mouse) were compared with homologous neurons from a non-model organism (rat). In this report, we have extended constellation pharmacology to the comparison of cellular subclasses in the CNS and PNS. In contrast to the DRG and TG neurons that transduce many different sensory modalities from the periphery to the brain, the VRC comprises neuronal networks with integrated physiological functions, i.e., cardiorespiratory control. Not surprisingly, the constellations of DRG cells are strikingly different from the constellations of VRC cells (Table 2).

In this study, we initiated the classification of different VRC cell types within the mouse brainstem at the level of the preBötC. We have identified three major cell classes: A, B, and C. Class A cells, on average, were strong responders to a depolarizing stimulus. The majority also responded to glutamate but not to any of the other receptor agonists tested in Fig. 1 (see Table 2). However, after preincubation with PNU, the majority of class A cells began to respond to ACh, indicating that they express α7 nAChRs (Fig. S3). In contrast to class A cells, class B cells, on average, were relatively weaker responders to a depolarizing

stimulus, and the majority of class B cells responded to several different receptor agonists (Fig. 1, Table 2, and Table S1). Class C cells either did not respond to a depolarizing stimulus or responded very weakly, suggesting that they include glial cells and potentially other nonneuronal cells (Fig. 1 and Table 2). A subset of class C cells (30%) responded to 0.2 mM $[K^+]_o$, suggesting that many of these cells are astrocytes (Fig. S2).

Within class B, the substance P-responsive neuronal subclasses are of particular interest because of their putative roles in generating the breathing pattern within the preBötC. Although the neurokinin-1 receptor does not discretely define the boundaries of the preBötC, histological studies demonstrate that neurokinin-1 receptors are highly concentrated at the level of the preBötC (27–29). Furthermore, the application of substance P to the preBötC stimulates rhythmic network activity and excitability of synaptically isolated preBötC neurons (16, 27). The two major subclasses of substance P-responsive neurons identified in dissociated cell culture (Table S1) appeared to be preBötC neurons because they responded to neuromodulators (substance P, ATP, and norepinephrine) previously shown to modulate the activity of inspiratory preBötC neurons (16, 30–32). Additionally, both subclasses responded to histamine, and one subclass responded to bradykinin (Table S1). Constellation pharmacology correctly predicted that preBötC neurons would include both bradykinin-insensitive and -sensitive cells (Figs. 1 and 3 and Table S1). Although previous work demonstrated a role for histamine H1 receptors in stimulating breathing (33), our study demonstrates that histamine directly stimulates inspiratory preBötC neurons. The impact of bradykinin on the excitability of preBötC neurons was unknown previously. Thus, we show that constellation pharmacology, coupled with investigations in more organized network structures, can provide insight into biologically relevant cell classifications and cell-specific neuromodulation.

A comparison of bradykinin and substance P responses in dissociated cells and in the brainstem slice revealed a similar distribution of bradykinin sensitivity when normalized to the substance P response of a given cell (Fig. 3*D*). About 28% of inspiratory neurons were relatively unaffected by bradykinin (with a <20% increase in firing rate; Fig. 3*C*); this lack of response could not be predicted by firing pattern (Fig. 3*B*). The proportion of inspiratory neurons unaffected by bradykinin was expected to be larger, given that ~50% of dissociated substance P-sensitive cells were unresponsive to bradykinin (Table S1). However, it may be that not all substance-P sensitive neurons in dissociated culture are preBötC neurons.

One way in which we will explore further the cell-specific constellations of VRC neurons is through the application of subtype-selective conotoxins. We have used this strategy to identify differences in the voltage-gated Na, Ca, and K channels expressed in two different subclasses of cold- and menthol-sensitive DRG neurons (5). The ever-expanding toolkit of selective pharmacological agents, including the conotoxins among many others, will make constellation pharmacology an increasingly powerful platform for single-cell profiling. With our approach we should be able to tease apart the differential physiological roles of divergent neuronal subclasses. By combining insights at the molecular and cellular level with insights at the network level, we hope to achieve a more integrated understanding of cardiorespiratory functions, including breathing-pattern generation and modulation, thus providing a test case that bridges molecular and systems neuroscience.

Materials and Methods

Materials and methods either have been described in detail previously (5–8, 21) or are described in *SI Materials and Methods*. Transverse medullary brainstem slices were taken from male and female P7–10 mice with a C57BL/6 background as described previously (21). All procedures in this study were approved by the Institutional Animal Care and Use Committees of the University of Utah or Seattle Children's Research Institute.

ACKNOWLEDGMENTS. We thank My Huynh for assistance in preparing the figures. This work was supported by Grant GM48677 from the National Institute of General Medical Sciences.

1. Bernard A, Sorensen SA, Lein ES (2009) Shifting the paradigm: New approaches for characterizing and classifying neurons. *Curr Opin Neurobiol* 19(5):530–536.
2. Nelson SB, Sugino K, Hempel CM (2006) The problem of neuronal cell types: A physiological genomics approach. *Trends Neurosci* 29(6):339–345.
3. Franco SJ, Müller U (2013) Shaping our minds: Stem and progenitor cell diversity in the mammalian neocortex. *Neuron* 77(1):19–34.
4. Sugino K, et al. (2006) Molecular taxonomy of major neuronal classes in the adult mouse forebrain. *Nat Neurosci* 9(1):99–107.
5. Teichert RW, et al. (2012) Characterization of two neuronal subclasses through constellation pharmacology. *Proc Natl Acad Sci USA* 109(31):12758–12763.
6. Teichert RW, et al. (2012) Functional profiling of neurons through cellular neuropharmacology. *Proc Natl Acad Sci USA* 109(5):1388–1395.
7. Smith NJ, et al. (2013) Comparative functional expression of nAChR subtypes in rodent DRG neurons. *Front Cell Neurosci* 7:225.
8. Teichert RW, Memon T, Aman JW, Olivera BM (2014) Using constellation pharmacology to define comprehensively a somatosensory neuronal subclass. *Proc Natl Acad Sci USA* 111(6):2319–2324.
9. Smith JC, Ellenberger HH, Ballanyi K, Richter DW, Feldman JL (1991) Pre-Bötzinger complex: A brainstem region that may generate respiratory rhythm in mammals. *Science* 254(5032):726–729.
10. Ramirez JM, Schwarzacher SW, Pierrefiche O, Olivera BM, Richter DW (1998) Selective lesioning of the cat pre-Bötzinger complex in vivo eliminates breathing but not gasping. *J Physiol* 507(Pt 3):895–907.
11. Tan W, et al. (2008) Silencing preBötzinger complex somatostatin-expressing neurons induces persistent apnea in awake rat. *Nat Neurosci* 11(5):538–540.
12. Gray PA, et al. (2010) Developmental origin of preBötzinger complex respiratory neurons. *J Neurosci* 30(44):14883–14895.
13. Ramirez JM, et al. (2012) The cellular building blocks of breathing. *Compr Physiol* 2(4): 2683–2731.
14. Gray R, Rajan AS, Radcliffe KA, Yakehiro M, Dani JA (1996) Hippocampal synaptic transmission enhanced by low concentrations of nicotine. *Nature* 383(6602):713–716.
15. Lieske SP, Thoby-Brisson M, Telgkamp P, Ramirez JM (2000) Reconfiguration of the neural network controlling multiple breathing patterns: Eupnea, sighs and gasps [see comment]. *Nat Neurosci* 3(6):600–607.
16. Peña F, Ramirez JM (2004) Substance P-mediated modulation of pacemaker properties in the mammalian respiratory network. *J Neurosci* 24(34):7549–7556.
17. Peña F, Parkis MA, Tryba AK, Ramirez JM (2004) Differential contribution of pacemaker properties to the generation of respiratory rhythms during normoxia and hypoxia. *Neuron* 43(1):105–117.
18. Zanella S, Roux JC, Viemari JC, Hilaire G (2006) Possible modulation of the mouse respiratory rhythm generator by A1/C1 neurones. *Respir Physiol Neurobiol* 153(2):126–138.
19. Dergacheva O, Griffioen KJ, Neff RA, Mendelowitz D (2010) Respiratory modulation of premotor cardiac vagal neurons in the brainstem. *Respir Physiol Neurobiol* 174(1-2):102–110.
20. Garcia AJ, 3rd, Koschnitzky JE, Dashevskiy T, Ramirez JM (2013) Cardiorespiratory coupling in health and disease. *Autonomic Neurosci* 175(1-2):26–37.
21. Ramirez JM, Quellmalz UJ, Richter DW (1996) Postnatal changes in the mammalian respiratory network as revealed by the transverse brainstem slice of mice. *J Physiol* 491(Pt 3):799–812.
22. Härtel K, et al. (2007) Calcium influx mediated by the inwardly rectifying K+ channel Kir4.1 (KCNJ10) at low external K+ concentration. *Cell Calcium* 42(3):271–280.
23. Härtel K, Schnell C, Hülsmann S (2009) Astrocytic calcium signals induced by neuromodulators via functional metabotropic receptors in the ventral respiratory group of neonatal mice. *Glia* 57(8):815–827.
24. Chen Y, Li G, Huang LY (2012) P2X7 receptors in satellite glial cells mediate high functional expression of P2X3 receptors in immature dorsal root ganglion neurons. *Mol Pain* 8:9.
25. Hone AJ, Meyer EL, McIntyre M, McIntosh JM (2012) Nicotinic acetylcholine receptors in dorsal root ganglion neurons include the alpha6beta4* subtype. *FASEB J* 26(2):917–926.
26. Whiteaker P, et al. (2007) Discovery, synthesis, and structure activity of a highly selective alpha7 nicotinic acetylcholine receptor antagonist. *Biochemistry* 46(22):6628–6638.
27. Gray PA, Rekling JC, Bocchiaro CM, Feldman JL (1999) Modulation of respiratory frequency by peptidergic input to rhythmogenic neurons in the preBötzinger complex. *Science* 286(5444):1566–1568.
28. Guyenet PG, Sevigny CP, Weston MC, Stornetta RL (2002) Neurokinin-1 receptor-expressing cells of the ventral respiratory group are functionally heterogeneous and predominantly glutamatergic. *J Neurosci* 22(9):3806–3816.
29. Pagliardini S, Ren J, Greer JJ (2003) Ontogeny of the pre-Bötzinger complex in perinatal rats. *J Neurosci* 23(29):9575–9584.
30. Doi A, Ramirez JM (2010) State-dependent interactions between excitatory neuromodulators in the neuronal control of breathing. *J Neurosci* 30(24):8251–8262.
31. Viemari JC, Garcia AJ, 3rd, Doi A, Ramirez JM (2011) Activation of alpha-2 noradrenergic receptors is critical for the generation of fictive eupnea and fictive gasping inspiratory activities in mammals in vitro. *Eur J Neurosci* 33(12):2228–2237.
32. Viemari JC, Ramirez JM (2006) Norepinephrine differentially modulates different types of respiratory pacemaker and nonpacemaker neurons. *J Neurophysiol* 95(4):2070–2082.
33. Qian ZB, Qi Y, Wu ZH (2010) [Histamine H1 receptors modulate the discharge activities of inspiratory neurons in the medial region of neonatal rat nucleus retrofacialis ex vivo]. *Nan fang yi ke da xue xue bao* [*Journal of Southern Medical University*] 30(1):54–56.